High-resolution spectroscopy on ground-state transitions of samarium-I

J. Mes[a], E.J. van Duijn, and W. Hogervorst

Laser Centre Vrije Universiteit, Department of Physics and Astronomy, De Boelelaan 1081, 1081 HV Amsterdam,
The Netherlands

Abstract. A high resolution laser-induced fluorescence study has been performed on thirteen ground-state transitions in samarium, using a frequency-doubled Ti:sapphire laser in the wavelength range 350–440 nm. From each spectrum isotope shifts and hyperfine structure constants A and B are derived. The results are used to determine the nuclear parameter $\lambda^{AA'}$.

PACS. 32.30.Jc Visible and ultraviolet spectra – 32.10.Fn Fine and hyperfine structure – 32.70.Jz Line shapes, widths, and shifts

1 Introduction

Samarium (Sm) is a rare-earth element with seven stable isotopes with the following abundances: ^{144}Sm 3.07%, ^{147}Sm 14.99%, ^{148}Sm 11.24%, ^{149}Sm 13.82%, ^{150}Sm 7.38%, ^{152}Sm 26.75% and ^{154}Sm 22.75%. Of these isotopes, ^{144}Sm and ^{152}Sm have recently obtained special interest in the field of cancer treatment. These isotopes become short lived radio isotopes ^{145}Sm and ^{153}Sm, after neutron absorption in a high flux reactor. The isotope ^{145}Sm has its application for brain tumor brachytherapy. The isotope ^{153}Sm is used for treatment of ocular cancer and for pain relief of bone cancer. Since there is not a simple method to enrich these isotopes using conventional techniques, e.g., ultra-centrifuges and calutrons, research towards a suitable spectroscopic route as the basis for laser isotope separation is of great interest.

In the past, spectra of Sm have been studied in detail in the 550 to 650 nm wavelength range [1–5] using dye- and diode-lasers. This has resulted in a wealth of accurate values of isotope shifts and hyperfine constants for the odd isotopes. Except for studies of Sm with UV laserdiodes [6], not so much is known about the higher lying states around 25 000 cm^{-1} for which UV light around 400 nm is required. In this energy region dye lasers are difficult to operate, but with the advent of powerful narrow-band frequency-doubled Ti:sapphire lasers this region has recently opened up.

We have performed high-resolution laser induced fluorescence experiments on ground-state transitions of Sm. To this end, a continuous-wave frequency-doubled Ti:sapphire laser was used covering a wavelength range between 350 and 440 nm. Thirteen transitions have been investigated, yielding isotope shift (IS) values, magnetic dipole constants A, and electric quadrupole constants B. From a King plot [7] analysis the nuclear parameter $\lambda^{AA'}$ (related to the change in mean square nuclear radii) is obtained for the various isotopes.

2 Experimental set-up

The experimental set-up is schematically depicted in Figure 1. Using this set-up laser-induced fluorescence (LIF) of Sm in the wavelength range from 350 nm up to 440 nm has been investigated. The light is generated by frequency doubling a narrow-band tunable cw Ti:S laser (Coherent 899-21). The Ti:S laser is pumped by a 10 W Nd:YVO$_4$ laser at 532 nm (Spectra Physics Millennia-Xs). The output of the Ti:S laser is coupled into a bowtie-shaped external enhancement cavity (EEC). This cavity contains a Brewster-cut nonlinear crystal for frequency doubling. The wavelength range of the EEC is limited by the phase-matching angle of the crystal and by the reflectance of the mirrors of the EEC. To cover the entire wavelength range of the Ti:S laser (700–900 nm), three LBO crystals are needed each cut at a different phase-matching angle. In Figure 2, the second harmonic output power of the EEC using an input power of 1.00 W at the fundamental wavelength, is plotted as a function of the wavelength for one of the LBO crystals used. This crystal is cut at angles of $\theta = 90°$, $\phi = 33.7°$ with respect to the optical axis and has a center wavelength of 780 nm. The other two LBO crystals used in the experiment are cut at $\theta = 90°$, $\phi = 37.8°$

[a] e-mail: mes@nat.vu.nl
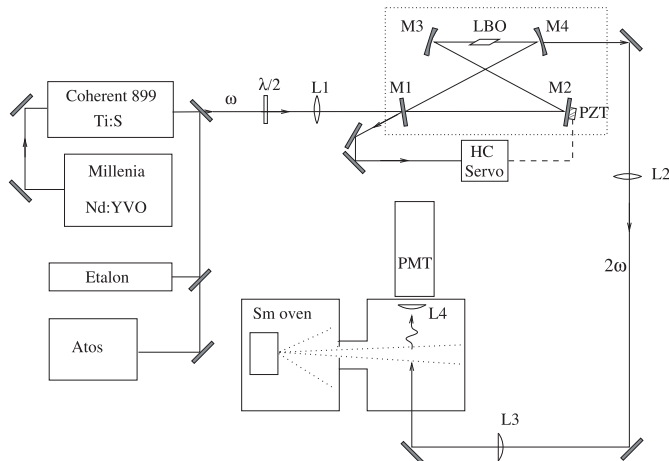
Fig. 1. Experimental set-up for the Sm laser-induced fluorescence experiment. L1: thin mode-matched lens. M1–M4: mirrors of external enhancement cavity, PZT: piezo-electric transducer for cavity locking, HC: Hänsch-Couillaud locking set-up, L2–L4: imaging lenses. The wavelength of the Ti:S laser is measured using a wavelength meter (ATOS) and an etalon.
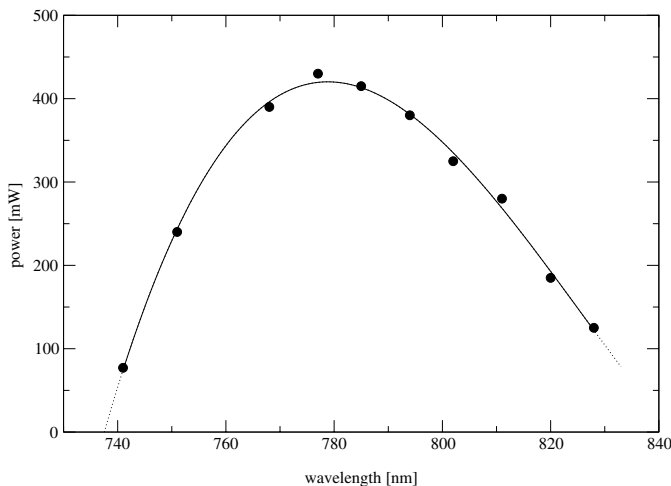
Fig. 2. Output power of the SHG set-up vs. wavelength using the LBO crystal cut at $\theta = 90°$, $\phi = 33.7°$. The fundamental power is 1 watt.

and $\theta = 90°$, $\phi = 27.0°$ respectively. Their center wavelengths are 744 nm and 850 nm, respectively. Mode matching of the Ti:S light into the EEC is performed by a thin lens L1. The cavity losses per round-trip are close to 1%, therefore the reflectivity of the input coupling mirror (M1) is chosen to be 99% to ensure impedance matching. This leads to a maximum coupling of 88% of the fundamental light into the EEC. The mirrors M3 and M4 have a reflectivity >99.8% and a radius of curvature of −75 mm to focus the beam in the LBO crystal. The distance between M3 and M4 is optimized for maximum conversion efficiency. To keep the EEC in resonance, the cavity is locked to the fundamental wavelength using the Hänsch-Couillaud locking technique [8] which supplies a feedback signal to the small ($\varnothing$6 mm × 2 mm) mirror M2 mounted on a piezo-electric transducer. The second harmonic light

is coupled out through M4 which is highly transparent (>97%) for the wavelengths 350 nm to 440 nm. From the full-width half-maximum of the cavity etalon peaks and the free spectral range a cavity finesse of about 310 is deduced. This leads to a cavity enhancement factor of 98. The bandwidth of the generated light is $\Gamma \lesssim 2$ MHz.

Since the transition $J = 0 \rightarrow J = 1$ at $26\,281.09$ cm^{-1} of Sm has a coincidental overlap with an O_2 absorption, the Ti:S laser and frequency doubling cavity are flushed with N_2 to ensure stable and mode-hop-free operation. During the spectroscopic experiment the absolute wavelength is measured using an ATOS wavemeter LM007, which has a short-term accuracy of 10^{-5}nm (≈ 5 MHz at 800 nm). A confocal etalon (FSR = 300 MHz and finesse ≈ 100) is used for a relative wavelength calibration.

A beam of Sm atoms is produced under vacuum conditions using a tantalum oven. This oven is heated by electron bombardment using a hot tungsten wire, through which a large current (typically 25 V/30 A) is run. Emitted electrons are accelerated towards the oven by an electric field of typically 2 kV/cm. Due to this electron bombardment the tantalum oven heats up to temperatures of about 1200 Kelvin. At this temperature a sufficiently dense atomic beam of Sm is produced. The atoms leave the oven through a small hole of 1.0 mm diameter. The laser beam intersects the atomic beam at a right angle some 60 cm downstream from the oven. Diaphragms are used in the atomic beam to reduce the Doppler broadening to ≈ 20 MHz. The background pressure in the vacuum system is about 5×10^{-7} mbar. The LIF light is imaged on a photomultiplier (PMT) sensitive in the UV, which is placed above the intersection region of atomic beam and laser beam.

3 Measurements

3.1 hyperfine structure

We have measured all known groundstate-transitions of Sm in the energy range of $22\,000$ cm^{-1} to $29\,000$ cm^{-1}. The even isotopes of Sm have no nuclear spin ($I = 0$), therefore the angular momentum J is the relevant quantum number. For the groundstate of Sm $J = 0$. The selection rules for optical transitions are $\Delta J = 0 \pm 1$, and $J = 0 \nrightarrow J = 0$. Hence, from the ground-state only transitions to excited states with angular momentum $J = 1$ are accessible.

The two odd isotopes of Sm, ^{147}Sm and ^{149}Sm, both have nuclear spin $I = 7/2$. Combined with angular momentum $J = 0$ in the ground-state of Sm only a single hyperfine level $F = 7/2$ results. In the excited state, however, $J = 1$, and the nuclear spin couples to the electron spin giving rise to a hyperfine splitting in three components with $F = 5/2$, $F = 7/2$ and $F = 9/2$ respectively. Therefore each spectrum will show 11 peaks, 5 for the even isotopes and 6 for the two odd isotopes. See upper graph in Figure 3. In some cases two or more peaks overlap (see lower graph in Fig. 3). In this case, the assignment of the peaks is more difficult. The observed linewidth varies
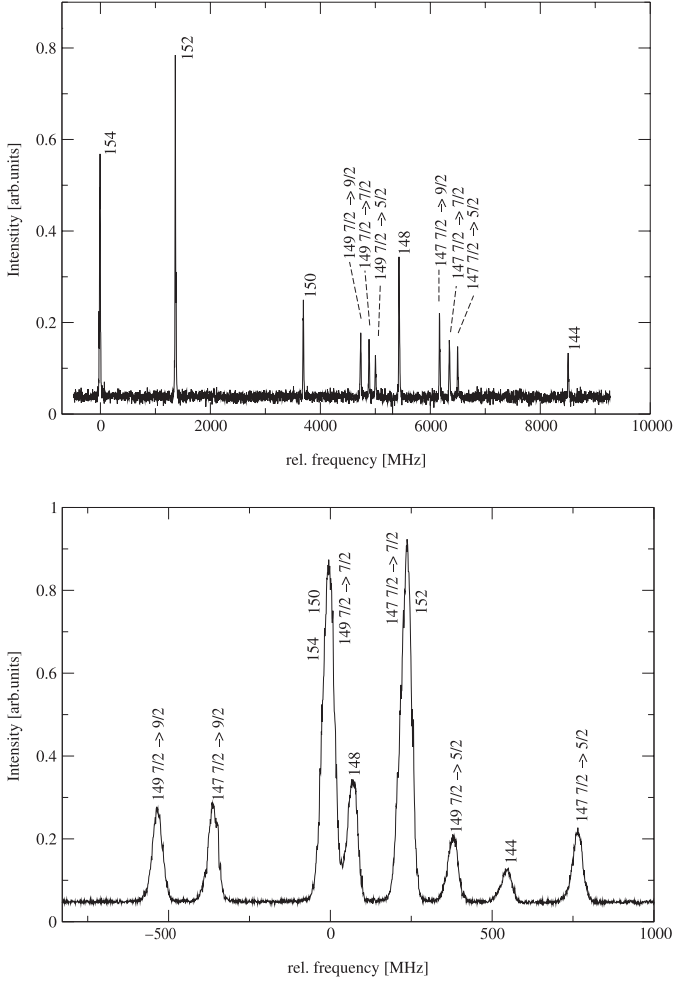
Fig. 3. Upper graph: a regular transition at $\lambda = 354.194$ nm, the ordering of the seven isotopes is as expected. Lower graph: the transition at $\lambda = 413.496$ nm. This is a more difficult to assign spectrum, resonances of different isotopes are overlapping and are not ordered "normally". When plotted in a King-plot, a line crossing the zero axis results. Note the different x-axis scale in both graphs.

between 15 and 50 MHz, depending on lifetime and transition strength of the transition.

The hyperfine shift contains two contributions. The first one results from the interaction of the nuclear magnetic moment μ_I with the magnetic field B_{el} due to the motion of the electrons around the nucleus. The second contribution is the interaction between the nuclear quadrupole moment Q_I and the electric field gradient q produced by the electrons. These contributions give rise to additional terms in the Hamiltonian of the atom

$$H_{hfs} = \mu_I B_{el} + Q_I q. \qquad (1)$$

The contributions to the atomic Hamiltonian are small and the energy contributions can be calculated using first order perturbation theory. This leads to [9,10]:

$$\Delta E_F(I, J, F) =$$
$$\frac{A}{2}C + \frac{B}{4}\frac{\frac{3}{2}C(C+1) - 2I(I+1)J(J+1)}{(2I-1)(2J-1)IJ}. \qquad (2)$$

ΔE_F gives the energy shift of the different hyperfine components of the odd isotope with respect to the centre-of-gravity-position in the spectrum. Here A is the magnetic dipole coupling constant, B the electric quadrupole coupling constant and C the Casimir factor

$$C = F(F+1) - I(I+1) - J(J+1). \qquad (3)$$

From the recorded spectra the position of each hyperfine component is determined. From this the centre of gravity of the odd isotope in the excited level can be derived as well as the hyperfine constants A and B. In Table 1 the constants for all excited levels as deduced from the investigated transitions are collected. An exception is the level at $26\,146.2$ cm^{-1}, where due to overlap with another transition starting from the first excited state at 292.6 cm^{-1}, it was impossible to determine the A and B values.

The ratio between the magnetic dipole constants A_{147}/A_{149} and the electric quadrupole constants B_{147}/B_{149} should be approximately constant for each transition. For Sm $A_{147}/A_{149} \cong 1.2$. However, in all measured transitions the electric quadrupole constants are small, resulting in a relatively large scatter in the ratio B_{147}/B_{149}. It can be seen from equations (4–6) that for the excited state of Sm in this case, the major contribution in ΔE_F originates from the magnetic dipole interaction and that the electric quadrupole constant has little influence on the energy shift

$$\Delta E_F(7/2, 1, 5/2) = -\frac{9A}{2} + \frac{15B}{28}, \qquad (4)$$

$$\Delta E_F(7/2, 1, 7/2) = -A - \frac{5B}{7}, \qquad (5)$$

$$\Delta E_F(7/2, 1, 9/2) = -\frac{14A}{4} + \frac{B}{4}. \qquad (6)$$

3.2 Isotope splitting

The observed isotope shifts (IS) in all measured transitions are collected in Table 2. The IS contains three components: the normal mass shift (NMS), the specific mass shift (SMS) and the field shift (FS):

$$\delta\nu_i = \delta\nu_{iNMS} + \delta\nu_{iSMS} + \delta\nu_{iFS}. \qquad (7)$$

The normal mass shift relates to the change in the reduced mass of electron and nucleus when comparing two isotopes (with mass-numbers A and A' respectively) and can be written as

$$\delta\nu_{iNMS} = M_{iNMS}\frac{A - A'}{AA'}, \qquad (8)$$

where

$$M_{iNMS} = \frac{\nu_i}{1822.8}. \qquad (9)$$

Table 1. Observed hyperfine constants A and B (in MHz) for the excited states of Sm as derived from the investigated transitions. For transition (a) at $\lambda = 382.465$ nm, the positions of the odd isotopes could not be determined.

wavelength [nm]	$E[\mathrm{cm}^{-1}]$	$A(149)$	$B(149)$	$A(147)$	$B(147)$
354.194	28233.1	$-33.41(24)$	$-0.84(27)$	$-41.05(3)$	$6.5(24)$
362.999	27548.3	$-100.5(5)$	$0.3(27)$	$-122.4(3)$	$-2.4(32)$
366.731	27267.9	$-83.36(8)$	$3.8(12)$	$-100.53(33)$	$-15.0(13)$
370.891	26962.1	$23.92(31)$	$-2.2(8)$	$28.6(5)$	$7.81(4)$
373.083	26803.7	$-307.1(2)$	$-0.5(12)$	$-372.8(4)$	$0.96(41)$
378.240	26438.2	$-106.26(1)$	$-5.8(9)$	$-128.6(3)$	$17.8(17)$
380.502	26281.1	$-85.5(18)$	$11.0(74)$	$-104.3(6)$	$-27.2(22)$
382.465^a	26146.2	.	.	.	.
410.246	24375.6	$-324.84(35)$	$2.1(30)$	$-394.88(9)$	$-15.4(4)$
413.496	24184.0	$-69.5(5)$	$-9.1(13)$	$-84.5(3)$	$19.5(11)$
423.191	23623.0	$-31.39(48)$	$1.0(7)$	$-37.6(3)$	$-9.8(12)$
430.222	23243.8	$-263.28(5)$	$1.72(3)$	$-319.40(26)$	$-8.49(8)$
436.413	22914.1	$-184.4(2)$	$-10.33(36)$	$-223.48(4)$	$32.6(5)$

Table 2. Observed isotope shifts (MHz) for the measured lines of Sm. The uncertainties are $\leq 0.6\%$. For the transition at $\lambda = 382.465$ nm, the positions of the odd isotopes could not be determined. Their positions have been obtained by interpolation of the King-plot.

wavelength [nm]	$154-152$	$152-150$	$150-149$	$150-148$	$148-147$	$148-144$
354.194	-1370.7	-2328.0	-1161.4	-1741.0	-878.8	-3074.7
362.999	-1141.8	-1857.7	-928.0	-1425.6	-719.1	-2552.6
366.731	-196.7	41.5	12.6	-129.6	-71.4	-417.0
370.891	1072.4	2408.4	1191.1	1552.4	774.5	2437.8
373.083	0.0	373.2	179.2	114.0	49.9	0.0
378.240	-387.8	-337.0	-174.6	-388.3	-201.4	-850.1
380.502	816.3	1866.3	932.7	1199.0	604.6	1863.0
382.465^a	674.5	1269.4	625.9^a	886.1	436.8^a	1513.1
410.246	-147.4	147.4	58.8	-69.5	-33.4	-307.9
413.496	-143.9	146.9	74.6	-48.4	-26.7	-286.6
423.191	-153.1	120.4	54.7	-72.1	-37.7	-315.9
430.222	1641.7	3532.2	1747.6	2322.2	1163.9	3724.7
436.413	-352.6	-484.2	-242.2	-409.9	-209.3	-783.8

Here ν_i is the frequency of the transition. The factor 1822.8 gives the ratio of proton and electron mass. The second term in equation (7) is the specific mass shift which is caused by correlations in the momenta of the electrons. In analogy to 8, the specific mass shift can be expressed as

$$\delta\nu_{iSMS} = M_{iSMS} \frac{A - A'}{AA'}. \qquad (10)$$

The exact value of the SMS is difficult to calculate, since the electronic wavefunctions have to be known. The third term in equation (7) is the field shift, which relates to the changes in the nuclear charge distributions when comparing the various isotopes

$$\delta\nu_{iFS} = E_i f(Z) \lambda^{AA'}. \qquad (11)$$

Here E_i is a factor related to the electron density at the nucleus, $f(Z)$ is a relativistic correction factor for the field shift. The nuclear parameter $\lambda^{AA'}$ is related to the change in mean-square nuclear charge radii when comparing the isotopes.

In a so-called King-plot [7] the measured isotope shifts for transition i are plotted in a particular way against the shifts in a reference transition j. For both transitions the shifts between adjacent isotope pairs are used (e.g. the shift between ^{154}Sm and ^{152}Sm). The plot then results in a straight line. When deviations occur, generally this indicates that the peaks in the measured transition have been wrongly assigned. For such a King-plot a reduced isotope shift (RIS) is used, which can be determined by subtracting the NMS from the measured isotope shift and by normalisation of the residual shift with respect to a reference isotope pair:

$$\delta\nu_{iRIS} = (\delta\nu_i - \delta\nu_{iNMS}) \left(\frac{AA'}{A - A'}\right) \left(\frac{A_{ref} - A'_{ref}}{A_{ref} A'_{ref}}\right). \qquad (12)$$

Table 3. Values of E_i/E_j, M_{iNMS}, M_{iSMS} and $F = E_i f(Z)$ derived from King-plots ($E_j = -0.285(\pm 4\%)$ and $f(Z) = 20.3$ GHz/fm^2).

wave l[nm]	E [cm^{-1}]	E_i/E_j	M_{iSMS}[THz]	M_{iNMS}[THz]	F
354.194	28 233.1	0.878 (6)	−3.37 (18)	464.92	5.08 (20)
362.999	27 548.3	0.655 (11)	−4.25 (22)	453.39	3.79 (12)
366.731	27 267.9	−0.0568 (19)	−5.86 (32)	448.82	−0.329 (18)
370.891	26 962.1	−1.2526 (29)	−6.64 (36)	444.82	−7.25 (29)
373.083	26 803.7	−0.364 (5)	−3.37 (18)	441.24	−2.11 (10)
378.240	26 438.2	−0.0585 (18)	−5.86 (32)	435.17	−0.339 (16)
380.502	26 281.1	−0.991 (9)	−5.65 (31)	433.11	−5.73 (24)
382.465	26 146.2	−0.554 (10)	−0.8778 (43)	430.33	−3.21 (12)
410.246	24 375.6	−0.280 (7)	−6.33 (35)	401.22	−1.62 (9)
413.496	24 184.0	0.286 (7)	−6.31 (35)	398.02	1.65 (9)
423.191	23 623.0	−0.2623 (14)	−6.07 (31)	389.08	−1.52 (6)
430.222	23 243.8	−1.77 (6)	−7.62 (42)	382.57	−10.24 (51)
436.413	22 914.1	0.1152 (10)	−2.78 (15)	377.14	0.667 (26)
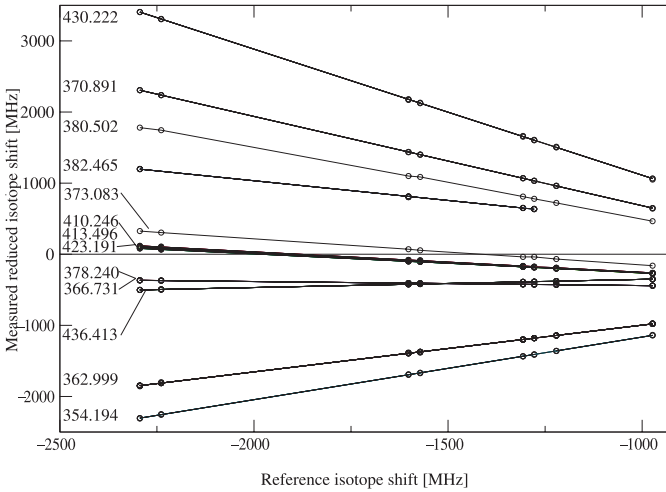
Fig. 4. King-plot, the obtained reduced isotope shifts are plotted against the reduced isotope shift of a transition at 636.74 nm measured by Jin et al. [3] The numbers in the graph are the wavelengths of the transitions in nm.

For the following analyses the isotope pair ^{154}Sm–^{152}Sm is used as reference pair, hence,

$$\delta\nu_{iRIS} = (\delta\nu_{iSMS} + E_i f(Z)\lambda) \left(\frac{AA'}{A-A'}\right) \left(\frac{2}{154 \times 152}\right). \tag{13}$$

The resulting normalised reduced isotope shift for each measurement i is now plotted against the reduced shifts of a reference line j in a King-plot, see Figure 4.

As a reference (x-axis), the measurement of the groundstate $J = 0 \rightarrow J = 1$, $4f^6 6s^2 \rightarrow 4f^6 6s6p$ transition at 636.74 nm by Jin et al. [3] was used. This transition has a large IS, the transition is nearly pure ($ns^2 - nsnp$), hence, the wavefunction has a relatively small admixture of other configurations. The lines in the King-plot can be

represented by

$$\delta\nu_{iRIS} = \frac{E_i}{E_j}\delta\nu_{jRIS} + \left(M_{iSMS} - \frac{E_i}{E_j}M_{jSMS}\right)\frac{2}{154 \times 152}. \tag{14}$$

The slope of the lines in the plot then gives E_i/E_j. Since E_j of the reference transition is known, E_i can be determined. The intercept of the lines with the vertical axis in the plot is

$$\left(M_{iSMS} - \frac{E_i}{E_j}M_{jSMS}\right)\frac{2}{154 \times 152}. \tag{15}$$

Since the reference transition is nearly pure $ns^2 - nsnp$, the M_{jSMS} factor of this transition is assumed to be zero, according to the semi-empirical relation [16]

$$\delta\nu_{iSMS} \cong (0 \pm 0.5)\nu_{iNMS}. \tag{16}$$

Therefore the intercept of the King-plot gives the value of $M_{iSMS}(\frac{2}{154 \times 152})$. From the value of this intercept $\delta\nu_{iSMS}$ then can be derived. From the observed isotope shift $\delta\nu_i$ and the also known $\delta\nu_{iNMS}$, the field shift for each isotope pair can be extracted. From the FS the values of the nuclear parameter $\lambda^{AA'}$ can be calculated using relation (11). The electronic factor E_i is determined from the King-plot. Brand et al. [11] derived that E_j has a value of -0.285 (with an uncertainty of 4%) for the $4f^6 6s^2 - 4f^6 6s6p$ transition of Sm I. The factor $f(Z)$ has a value of 20.3 GHz/fm^2 for a uniformly charged sphere, according to Babushkin [12]. In Table 3 the values of E_i/E_j, M_{iNMS}, M_{iSMS} and $F = E_i f(Z)$ as derived from King-plots are collected.

4 Discussion

The results of the King-plot analyses are collected in the Tables 3 and 4. From the King-plot (Fig. 4) some further qualitative conclusions can be drawn. The slope of the

Table 4. Average values of the nuclear parameter $\lambda^{AA'}$ calculated from our experiments and the values obtained in electron-scattering experiments from reference [14]. The error is mainly determined by the uncertainty in E_j and $f(Z)$.

AA'	$\lambda^{AA'}$ [fm^2]	$\lambda^{AA'}$ [fm^2] Ref. [14]
$154-152$	0.220 (14)	0.221 (14)
$152-150$	0.407 (27)	0.411 (27)
$150-149$	0.202 (12)	0.224 (12)
$150-148$	0.291 (15)	0.303 (15)
$148-147$	0.147 (8)	0.171 (8)
$148-144$	0.497 (24)	0.478 (24)

lines, which varies from positive to negative, is determined by the ratio E_i/E_j (see Eq. (14)), so all overlapping lines have similar electronic structure in the excited state (since they all connect to the same ground-state). In Sm two electronic configurations are relevant and may be mixed in the excited states: $4f^6snp$ and $4f^55d6s^2$. In a King-plot with as reference a pure $4f^66s^2 \rightarrow 4f^66s6p$ transition, a positive slope indicates a dominant $4f^55d6s6p$ character of the excited state, whereas the negative slope must be attributed to more dominant contributions of the $4f^55d6s^2$ configuration. This is confirmed by the information on the atomic spectra database of the NIST [13], indicating that the excited states involved in the transitions at 380.502 nm and 430.222 nm have respectively a dominant $4f^55d6s^2$ ^{7}F and $4f^55d6s^2$ ^{7}G character (see Fig. 4). Without quantitative information on the value of E_i for a pure $4f^55d6s^2$ configuration it is not possible to analyse the slopes of the King-plot in more detail.

For the observed transition at $\lambda = 382.465$ nm (level at $26\,146.0$ cm^{-1}) the odd isotopes could not be assigned since the spectrum shows many weak lines. This is due to overlap with a transition starting from the first metastable state at 292.58 cm^{-1} to the $4f^55d6s^2$ ^{9}H level at $26\,438.25$ cm^{-1}. The positions of the odd isotopes are determined by interpolation of the King-plot. One transition reported in literature (at $26\,910$ cm^{-1} [13]) could not be observed in our experiment, even at very high atom density.

Regarding the nuclear parameter, it could be argued that the exact value of the SMS of the reference transition is an approximation. It would make more sense to use the $\lambda^{AA'}$ data from electronic scattering experiments [14] to determine the FS and obtain in this way information on the value of the SMS. Blaum et al. [15] used this approach to test the approximation $\delta\nu_{iSMS} \cong (0 \pm 0.5)\delta\nu_{iNMS}$ [16] for a pure $ns^2 - nsnp$ transition in case of gadolinium. It turned out that for their case the approximation $\delta\nu_{iSMS} \cong 0$ was not really correct. We have also tested this approach here. However, the electronic scattering experiments on Sm yield values of $\lambda^{AA'}$ with large uncertainties.

Extrapolation of the lines in a King-plot based on these data to determine the intercept would not yield more precise values for the SMS.

5 Conclusion

We report on high resolution measurement of Sm-I transitions from the $J = 0$ ground-state to $J = 1$ excited states in the $23\,000$–$29\,000$ cm^{-1} energy range. One reported line (at $26\,910$ cm^{-1} [13]) could not be observed in our experiment even at high atom density. The values of the nuclear parameter $\lambda^{AA'}$, obtained from our measurements agree with the results from Jin et al. [3] and the data from muonic and electron scattering experiments [14].

References

1. H. Brand, B. Nottbeck, H.H. Schulz, A. Steudel, J. Phys. B **11**, 99 (1977)
2. J.A.R. Griffith, G.R. Isaak, R. New, M.P. Ralls, C.P. van Zyl, J. Phys. B: At. Mol. Phys. **12**, L1 (1979)
3. W.G. Jin, T. Horiguchi, W.Yang, I. Endo, Phys. Rev. A **49**, 6 (1994) 4398
4. T. Kobayashi, I. Endo, A. Fukumi, T. Horiguchi, Y. Ishida, T. Kondo, T. Kuwamoto, N. Mimamoto, T. Nakamura, T. Takahashi, Z. Phys. D **39**, 209 (1997)
5. A. Fukumi, I. Endo, Z. Phys. D **42**, 243 (1997)
6. H. Park, D. Kwon, Y. Rhee, J. Opt. Soc. Am. B **21**, 1250 (2004)
7. W.H. King, *Isotope Shifts in Atomic Spectra* (Plenum Press, New York/London, 1984)
8. T.W. Hänsch, B. Couillaud, Opt. Commun. **35**, 441 (1980)
9. H. Kopfermann, *Nuclear moments* (Academic Press, New York, 1958)
10. G.K. Woodgate, *Elementary Atomic Structure*, 2nd edn. (Oxford University Press, Oxford, 1989)
11. H. Brand, B. Seibert, A. Steudel, Z. Phys. A **296**, 281 (1980)
12. R. Babushkin, Phys. Rev. **188**, 1916 (1969)
13. Atomic-Spectra-Data-Base on website of NIST, address: http://physics.nist.gov/PhysRefData/ contents-atomic.html
14. G. Fricke, C. Bernardt, K. Heilig, L.A. Schaller, L. Schellenberg, E.B. Shera, C.W. De Jager, At. Data Nucl. Data Tables **60**, 117 (1995)
15. K. Blaum B.A. Bushaw, S. Diel, Ch. Geppert, A. Kuschnick, P. Muller, W. Nortershauser, A. Schmitt, K. Wendt, Eur. Phys. J. D **11**, 37 (2000)
16. K. Heilig, A. Steudel, At. Data Nucl. Data Tables **14**, 613 (1974)